Surface & Coatings Technology 205 (2010) 2393–2403

Contents lists available at ScienceDirect

Surface & Coatings Technology

journal homepage: www.elsevier.com/locate/surfcoat

Residual stress evaluation at the micrometer scale: Analysis of thin coatings by FIB milling and digital image correlation

Alexander M. Korsunsky [a,*], Marco Sebastiani [b], Edoardo Bemporad [b]

[a] Dept. of Engineering Science, Univ. of Oxford, Parks Road, Oxford OX1 3PJ, United Kingdom
[b] University of Rome "ROMA TRE", Mechanical and Industrial Engineering Department, Via Vasca Navale 79, 00146 Rome, Italy

ARTICLE INFO

Article history:
Received 25 June 2010
Accepted in revised form 18 September 2010
Available online 25 September 2010

Keywords:
Residual stresses
Focused ion beam (FIB)
Digital image correlation (DIC)
Finite element modeling (FEM)
Coatings

ABSTRACT

In this report, an optimised method for residual stress determination at the microscopic scale is presented. The newly proposed approach involves incremental Focused Ion Beam (FIB) milling of annular trenches at material surface, combined with high resolution SEM imaging of a previously deposited marker pattern. Digital image correlation (DIC) analysis of the relative displacements between markers with respect to the undisturbed state provides a measure of strain relief. Results of finite element modeling show that the proposed configuration gives complete strain relief when the annular trench depth becomes comparable with the diameter of the remaining stub, thus allowing analytical calculation of the average residual stress from measured strain components. Basing on results of modeling, the experimental methodology has been developed and optimised for residual stress analysis in thin coatings. In order to cover a wide range of material properties and residual stress states, two different materials have been selected: TiN CAE-PVD coating (hard and stiff, with compressive residual stress) on WC–Co substrate, and also an Au MS-PVD coating (soft and compliant, with tensile residual stress). The procedure for the optimization of FIB milling parameters is reported. Results are validated by comparison with residual stress evaluation by X-ray diffraction and curvature measurement on the two different specifically selected PVD coatings.

1. Introduction

Residual stresses play a crucial role in determining the deformation behaviour and performance of engineering components and materials, from bulk alloys and composites used in construction and manufacturing industries down to micro-mechanical MEMS/NEMS systems and the stresses within individual grains of polycrystalline aggregates, thin films and coatings. Residual stresses exist across the scales, from macro- to nano-, and their evaluation must necessarily be performed using appropriately sized probes. The traditional methods of residual stress evaluation are limited in their spatial resolution to fractions of a millimetre, making them ill-suited to the study of e.g. intragranular stresses in polycrystalline systems with the grain size of a few micrometers.

On the other hand, the rapid development of nano-science and nano-technology in recent decades calls for the development of appropriate nano-scale (or at least sub-micron) analysis tools for residual stress evaluation [1–5]. The applications where (sub)micron-scale residual stress measurement is in demand include nano-structures, nano-devices and nano-structured materials. A portable and accessible residual stress methodology should be applicable not only in research context, but preferably be reducible to procedures that would allow routine use in industry, including in the context of production and quality control.

Residual stress evaluation techniques can be classified into non-destructive techniques, such as X-ray and neutron diffraction, and destructive and semi-destructive methods that involve material removal and the measurement of consequent surface strain relief.

The spatial resolution of the classical methods of residual stress evaluation by X-ray diffraction using laboratory sources is limited to a fraction of a millimetre. In most cases this is insufficient for the study of intragranular stresses. X-ray beams that are many orders of magnitude better in terms of flux and parallelism are produced at synchrotrons.

In recent years the development of micro-focus synchrotron X-ray beams has opened the way for stress evaluation at the micron and sub-micron scales. The key to the possibility of using this approach is the availability of high intensity, high brightness, micro-focus polychromatic X-ray beams only produced at third generation synchrotron sources. X-ray beams generated by a bending magnet or an insertion device such as a wiggler or wavelength shifter are focused on the sample by the use of Kirkpatrick–Baez (KB) achromatic mirrors, allowing the creation of beam spot on the sample less than 100 nm in diameter. The wide bandwidth of the incident beam ensures that the interaction between the incident beam and the

* Corresponding author. Tel.: +44 1865 273043; fax: +44 1865 273010.
E-mail address: alexander.korsunsky@eng.ox.ac.uk (A.M. Korsunsky).

0257-8972/$ – see front matter © 2010 Elsevier B.V. All rights reserved.
doi:10.1016/j.surfcoat.2010.09.033

crystalline gauge volume leads to the creation of a Laue diffraction pattern on a 2D detector. Data collection can be conducted in both the reflection and transmission geometries. The analysis of the diffraction pattern allows simultaneous determination of the orientation and lattice parameters of the crystal(s) present within the gauge volume. Further details of this technique and its implementation can be found in the literature [1,2].

One of the limitations of synchrotron-based micro-beam Laue technique for the measurement of residual stresses in (sub)micrometer-sized volumes is the restricted access to synchrotron instruments, making the use of this technique difficult for routine industrially-motivated analysis.

The purpose of the present study was to consider the possibility of developing a portable and flexible semi-destructive method that would be applicable down to the microscopic scale, and would allow routine determination of residual stresses in a variety of single and poly-crystals using the combination of focused ion beam (FIB) milling, SEM imaging, digital image correlation (DIC) analysis, and finite element modeling (FEM).

In the context of microscopic residual stress evaluation, focused ion beam (FIB) provides a natural choice of the machining tool. Similarly, scanning electron microscopy (SEM) offers excellent imaging resolution for input into digital image correlation analysis. Based on this reasoning, dual beam FIB-SEM system was chosen as the instrumental base for the implementation of the new method.

Prior attempts at the development of such techniques involved the use of FIB milling as the micro-scale machining tool; and various methods of strain measurement, notably Moiré interferometry [5] and digital image correlation (DIC) [6]. Sabate et al. [6] used FIB to machine straight shallow or deep trenches within the sample surface. Analytical solutions for the displacement fields around a crack taken from linear elastic fracture mechanics were used to estimate the residual stress component in the direction perpendicular to the trench extension. Results have been presented for the cases of silicon wafers and coated systems [7,8].

Massl et al. [9] proposed a cantilever method for the determination of residual stress depth profiles in thin films by measuring the deflection of a FIB-fabricated micro-cantilever, as a function of the gradually reduced film thickness. The main limitation of this approach is that the micro-cantilever must be necessarily fabricated in the proximity of the specimen edge, or near a previously fractured surface, making it unsuitable for micro-scale residual stress mapping, e.g. for intragranular stress analysis in polycrystalline materials, or stress measurement in thin films on metallic substrate.

However, strong limitations are still present for these adopted geometries, in particular:

- None of the selected geometries allows to do in situ testing with sufficient spatial resolution (i.e. lower than 1 μm);
- In the case of hole and slot geometries, strain gradients are always present in the proximity of the milled region. Furthermore, the maximum amount of strain relief always takes place in the vicinity of the FIB-damaged area;
- In the case of the slot-milling and blind hole drilling geometries, FEM modeling is required for residual stress calculation after relaxation strain measurement;
- The micro-cantilever method can be realized only at the sample edge, and only in the case of coatings on brittle substrates;
- In the case of slot-milling and the micro-cantilever method, only one stress component can be evaluated.

In this work, we propose an innovative geometry for the FIB milling experiment, which involves incremental focused ion beam (FIB) milling of annular trenches at material surface (Fig. 1). This method is intended to give complete information on the in-plane residual strain components when applied in combination with high resolution SEM imaging of a previously deposited marker pattern and Digital Image Correlation (DIC) analysis of the relative displacements between markers with respect to the undisturbed state.

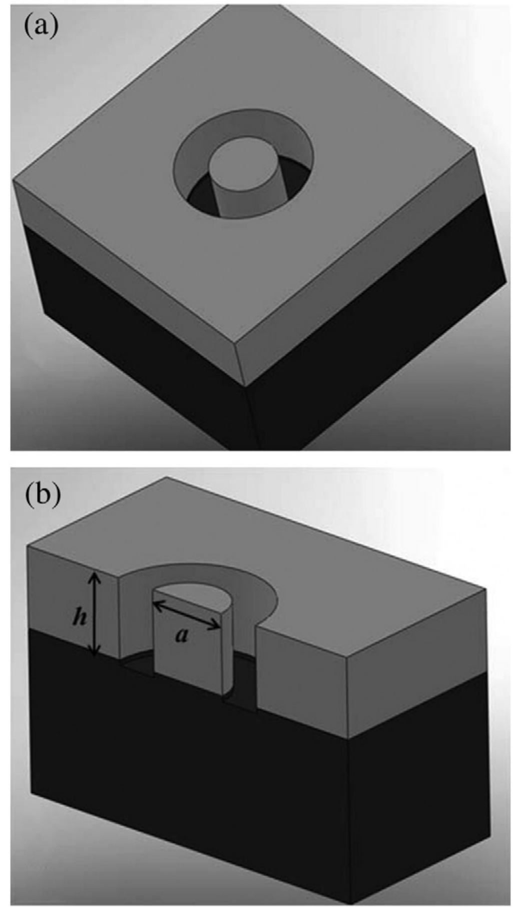

Fig. 1. Illustration of the principle of ring drilling, and the idealised geometry of the remaining "stub".

There exists an important additional advantage of the proposed configuration. The surface of the "stub" is not subjected to machining operation, and under careful cutting should remain substantially undisturbed. This situation lends itself naturally to strain measurement using digital image correlation. If a pattern of at least three non-collinear markers is deposited on the sample surface prior to ring drilling, then three independent components of strain can be determined, and the complete two-dimensional characterisation of the strain relief be obtained.

The proposed approach shares many common features with macroscopic incremental hole drilling, and admits calibration using substantially similar approaches using finite element modeling for influence coefficient evaluation [10]. Analytical solutions for the eigenstrain influence functions have also been derived [11,12].

It is important to note that, in contrast with the hole drilling situation, where strain relief around the drilled hole is always partial and position-dependent, in the present configuration the relieved strain state at material surface can be assumed to be to a good approximation uniform; and complete strain relief can be assumed to take place once a certain drilling depth is reached. This ensures maximum sensitivity of the newly proposed method to pre-existing residual stress.

In this work, finite element modeling (FEM) has been adopted to investigate the relaxation strain profile during incremental ring-core milling of a residually stressed coated surface, with the main objective of identify the optimal geometrical configuration for strain analysis, in terms of stub's diameter and milling depth.

The experimental implementation of the ring drilling technique on thin coatings using the dual beam FIB-SEM system is then described. The selection of the method for surface patterning is discussed, along with the choice of ring drilling conditions.

Next, the application of digital image correlation analysis to the determination of strain relief due to ring drilling is described. Stress evaluation is achieved by comparison between FEM predictions for strain relief, on the one hand, and the experimentally determined incremental strain relief measured by digital image correlation on the other.

Finally, the results are reviewed and discussed, and comments are made on the likely future developments of the novel approach proposed here.

2. Modeling strain relief from an annular trench

In preparation for the experimental implementation of FIB ring drilling method for micro-scale residual stress analysis, finite element simulation of the surface strain relief due to incremental ring-core milling over a residually stressed coated system has been carried out.

Relaxation strain after milling of annular trenches has been already studied in the past by Finite Element Modeling for the case of the macro-scale ring-core method [13,14].

In this case, the main objective of the FEM modeling was to identify the optimal geometrical conditions (i.e. size and depth of the trench) for the application of the ring-core geometry to residual stress analysis at the micro-scale on thin coatings.

The details on the FEM procedure adopted in this work and the basic equations of stress gradient analysis by the incremental ring-core method are reported in Appendix A.

In the following, the results are presented for the case of an equi-biaxial residual stress field (Eq. (A5), see Appendix A). This situation was chosen because it is particularly relevant for the case of thin coatings on homogeneous substrate.

Fig. 2 illustrates the plot of computed strain relief curve for the case of equi-biaxial constant through the thickness stress field (as calculated by Eq. (A5)) for all the material properties combinations considered here ($d/t = 1$), and then normalised with respect to the biaxial modulus $E/(1-\nu)$) vs the trench depth normalised with respect to the stub diameter (h/d). A unique master relaxation curve was found to apply for all material property combinations considered in this work. Another important observation is that the normalized stress relief approaches unity for $h/d > 1$, meaning that full stress relief (i.e. complete saturation) is achieved when the trench depth is at least equal to its diameter.

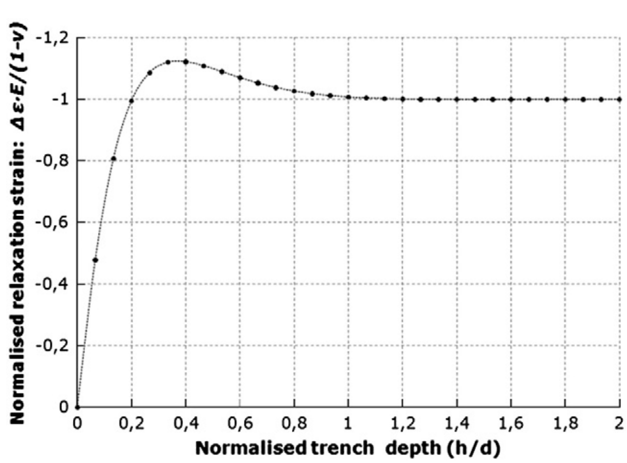

Fig. 2. FEM modeled normalized stress relief as a function of normalized drilling depth.

This observation was made for all material property combinations, showing that complete saturation is achieved for $h/d > 1$ independently of the elastic properties of the substrate.

It is important to note that the above conclusions are valid provided the stub diameter (d) is equal to, or is smaller than the coating thickness (t). In case of $d/t > 1$, a dependence of the relief strain profile on the elastic properties of the substrate may be observed.

It is also worth noting that relief strain was found to be nearly uniform over the surface of the stub, as expected. This situation is significantly different from the conventional hole drilling geometry, where strain gradients are present in the vicinity of the edge of the hole. This aspect is particularly relevant in the case of FIB milling, since the edges of the milled area are usually damaged by the ion beam and by material re-deposition effects [6,7].

We can then conclude that the measured strain relief $\Delta\tilde{\varepsilon} = \Delta\varepsilon(h)|_{h \geq d}$ between the original (undisturbed) surface and the fully relieved surface of the stub of diameter d provides information about the average residual stress σ^* within the sample surface without any further need for Finite Element Modeling. When complete strain relief $\Delta\tilde{\varepsilon}$ is achieved, the equi-biaxial residual stress is simply found from

$$\tilde{\sigma} = -\frac{E\Delta\tilde{\varepsilon}}{(1-\nu)}. \tag{1}$$

For the consideration of non-equi-biaxial residual stress states, the residual stresses are written in terms of maximum strain reliefs $\Delta\tilde{\varepsilon}_1$, $\Delta\tilde{\varepsilon}_2$ as follows:

$$\begin{aligned} \tilde{\sigma}_1 &= -\frac{E}{(1-\nu^2)}\left[\Delta\tilde{\varepsilon}_1 + \nu\Delta\tilde{\varepsilon}_2\right] \\ \tilde{\sigma}_2 &= -\frac{E}{(1-\nu^2)}\left[\Delta\tilde{\varepsilon}_2 + \nu\Delta\tilde{\varepsilon}_1\right] \end{aligned} \tag{2}$$

Here indices “1” and “2” refer to the principal stress (and strain) directions at sample surface.

This result is very relevant in the field of residual stress measurement of thin films, an observation that has not been made in previous studies on the conventional ring-core method.

When the directions of the principal stresses are not known a priori, strain should be measured along three different directions and the in-plane principal stress components should be calculated by the Mohr's circle, as usually performed in macro-scale hole drilling and ring-core methods.

It is important to remind that the simplified Eqs. (1–2) hold when the geometry of the FIB-milled trench is close to the ideal one shown in Fig. 2.

Fig. 3 reports the normalized relaxation strain profile for the case of the lateral slope of the stub being equal to 9°, in comparison with the analogous curve obtained for the ideal case. The results show that a slight difference exists between the two cases, with the relaxation curve being steeper in the ideal case. The actual slope of the stub should be therefore measured in the experimental practice and then corrected in the model. However, the observation that full saturation of strain relief is reached for $h/d > 1$ remains valid also in case of this lateral slope being present, so that the use of Eqs. (1–2) can still be considered appropriate, provided the lateral slope of the stub does not exceed about 10°.

It is interesting to observe that the stress relief curve in Fig. 2 also displays a maximum. This maximum relief has the relative magnitude

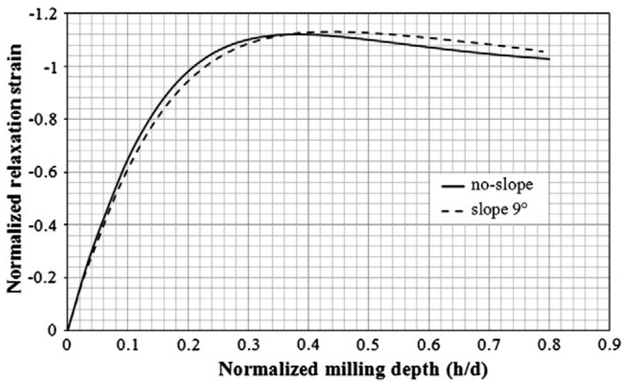

Fig. 3. FEM modeling of the influence of lateral on relaxation strain profile during ring-milling over a residually stressed surface.

of 1.125 and corresponds to the relative trench depth of h/d~0.4, independently of the mechanical properties of the coating and substrate. At greater drilling depths the magnitude of the relaxation strain begins to decrease until full saturation is reached. This interesting phenomenon is likely to be associated with the Poisson effect, and deserves further detailed investigation. It is also worth noting that full relief is first achieved at relative drilling depth of only about $h/d = 0.2$. If this modeling result is validated experimentally, it may provide an important practical short-cut for the implementation of this residual stress evaluation technique.

The observed shape of the relaxation curve explains why the normalized trench depth h/d is usually limited to about 0.3–0.4 for the conventional incremental ring-core method [13,14], due to the loss of sensitivity to stress gradients at higher milling depths.

The following main conclusions can be finally drawn from the modeling activities described here:

1. Ring-core milling over a residually stressed surface allows full stress relaxation over the stub surface for $h/d \geq 1$ (i.e. aspect ratio of the stub ≥ 1), meaning that average residual stress field can be easily computed by Eqs. (1–2), thus avoiding any further need of FEM modeling;
2. In case of thin films, this results is also independent on substrate's elastic properties, if the stub's diameter is equal to (or lower than) coating thickness (so no need of FEM modeling also for coatings)
3. The computed relaxation strain was found to be uniform over the surface of the stub, in contrast to what usually happens for the hole drilling geometry.
4. On the other hand, when measurements are performed with the main aim of investigating depth gradients of stress, the shape of the measured relaxation strain suggests that FIB ring drilling should be divided into many small depth increments up to a maximum normalized trench depth h/d~0.4; in this case, residual stress can be calculated by Eq. (A2) after FEM analysis of calibration coefficient matrices A_{ni} and B_{ni} (see Appendix A), following the procedure for stress profiling conventionally used for the macro-scale hole drilling and ring-core methods.

These conclusions drawn from the finite element modeling study confirm that the micro-scale ring-core approach should be well-suited to the study of residual stress states with (sub)micron resolution, provided it can be implemented practically by means of FIB ring drilling to the depths at least equal to the diameter of the remaining stub (also equal to coating thickness in case of stress measurement in thin films). This should be followed by the measurement of relief strain by high resolution SEM imaging and Digital Image Correlation (DIC) analysis.

2.1. Introduction of a material independent "master curve" for average stress calculation by the ring-core method

In order to aid the interpretation further we develop here a practically convenient analytical approach to the data interpretation based on the FE modeling results. For biaxial residual stress that remains constant with depth, the shape of the strain relief curve was found to be universal, i.e. independent of the properties of the sample being studied, as reported in Fig. 2. This conclusion applied even when the sample consisted of a coating layer on a dissimilar substrate, provided that the stub diameter is kept close to the coating thickness value. This is a very strong result, since it makes it possible to describe the shape of the master curve by a simple approximating function. Such function should allow scaling in terms of the maximum strain relief magnitude, and also in terms of the depth normalization constant (in our case chosen to be the inner ring radius). Once such simple functional form was found, the procedure for residual stress evaluation should involve:

(i) Fitting the master curve function to the experimental data
(ii) Determining the value of the maximum relief strain, and its uncertainty
(iii) Computing the residual stress value using Eq. (3).

The approximating master function is indicated in Fig. 4 by the continuous curve, while the FE calculation results are plotted using the dashed line. The formula for the master function is also indicated in the figure. The master function is expressed in terms of the normalized depth parameter $z = (x/0.42d)$, where x is the drilling depth and d is the outer diameter of the remaining stub. The complete relief strain $\Delta\tilde{\varepsilon}$ is contained in the master function expression as a scaling parameter.

Effectively, we now have a simple analytical expression that encapsulates all the results of the FE simulation in simple and compact form. Note that the formula is valid within the range of interest of normalized depths up to the value of 2.

3. Experimental implementation

3.1. Deposition of coatings and preliminary characterisation

The materials used in the present study were a 3.8 μm TiN coating deposited on the WC–Co substrate by cathodic arc evaporation physical vapour deposition (CAE-PVD) and a 1.5 μm Au coating on Si/SiO_2 substrate deposited by DC sputtering PVD technique (voltage 410 V, current 0.2 A). The deposition parameters for the TiN coating are reported in [15]. The microstructures of both coatings are illustrated in Fig. 5a–b.

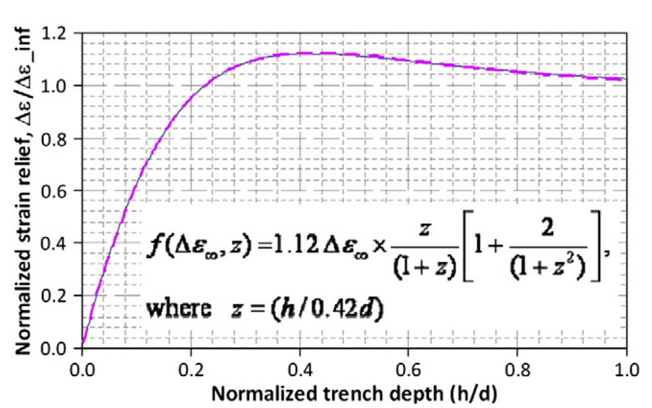

Fig. 4. Normalized stress relief as a function of normalized drilling depth (dashed curve — FE model; continuous curve — "master function" approximation).

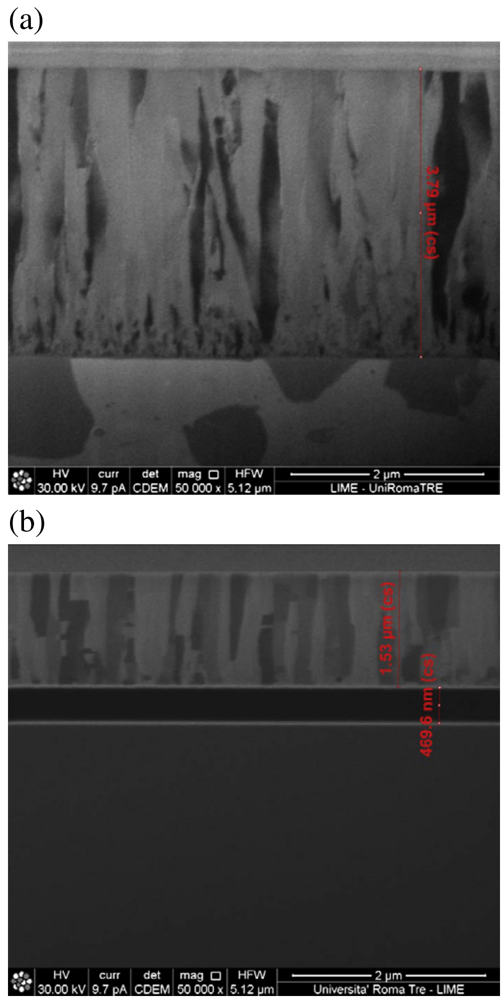

Fig. 5. Microstructures of the (a) the TiN coating on WC–Co substrate and (b) the Au coating on Silicon substrate.

The two coated systems were selected in order to perform a quantitative estimation of the resolution and sensitivity of the proposed technique for two distinct cases of soft-ductile and hard-brittle materials, where a transition from tensile to compressive residual stress is also expected.

The intrinsic hardness and elastic modulus of the two PVD coatings were measured by means of nano-indentation (NanoIndenter G200 — Agilent technologies). Continuous Stiffness Measurement (CSM) method was used with a Berkovich indenter tip calibrated on certified fused silica reference sample at 200 nm maximum penetration depth, $0.05\ s^{-1}$ constant strain rate, 10 s hold at peak load for creep correction, and 45 s hold at 90% for thermal drift correction. The Oliver and Pharr method [16] was adopted for hardness and elastic modulus evaluation. Other test parameters were in accordance with the 14577-1-2 ISO standards.

An average indentation modulus of 503 ± 25 GPa for the TiN coating and 74.5 ± 7 GPa for the Au coating, respectively, were measured at a penetration depth of 80 nm (Poisson's ratios being taken from literature for both materials). Correction for pile-up was adopted in the case of the Au coating by direct SEM contact area measurement after nano-indentation testing.

The average residual stress inside the TiN coating was separately measured using a D/max-RAPID Rigaku microdiffractometer with Cu Kα radiation, equipped with a cylindrical image plate (IP) detector and using a collimator diameter of 300 μm. Residual stresses were calculated by the analysis of a single Debye ring and then using the conventional d-$\sin^2\psi$ plot to calculate the average stress in the coating [17].

The residual stress state on the Au PVD coating was also measured by the curvature measurement and application of the Stoney equation [18].

3.2. Implementation of the FIB ring-drill procedure

In all cases, a thin platinum layer was deposited on the sample surface by focused ion beam deposition. The function of this additional layer is to protect the sample surface during ring drilling, and to provide the surface for the creation of the displacement analysis pattern via FIB milling.

As shown in Fig. 6a, a regular grid of small dots (diameter and depth of about 60 nm) was milled in the platinum layer. A high resolution SEM micrograph of the pattern was acquired before ring drilling (Fig. 6b), and in a step-wise fashion during the ring drilling experiment (Fig. 6b–c). Particular care was taken at all times to avoid the artefacts in displacement measurement that may be induced by electron beam drift during SEM image acquisition.

By using high image resolution (up to 4096×3775 pixels) and decreasing the scanning dwell time down to 1 μs, acceptable reliability of digital image acquisition was achieved. This manifested itself in the absence of significant errors in the imaging of a calibrated object, i.e. errors were maintained at levels lower than the nominal resolution of the SEM column at the magnification used. Quantitative interpretation of the images in the fast scanning direction delivered the best dimensional accuracy, while an error of about 0.2% (corresponding to the drift of 2 nm for a field of view of 1 μm) was observed when length measurement was performed in the slow scanning direction (vertical direction in Fig. 6b). Based on these observations, and in order to obtain consistent quantitative information about biaxial strain relaxation, the in-plane displacement components over the surface area of the stub were evaluated from images obtained by rotating the sample stage to three fixed positions (0°, 45° and 90°) and acquiring three different micrographs at each milling step. Displacement components were evaluated in the fast scanning electron beam direction in each case.

The approach adopted allows one to use the equations for stress calculation that are already available for the macro-scale hole drilling and ring-core methods.

FIB ring-core milling was performed at the current of 48 pA and the voltage of 30 kV at the incremental milling depth step of 200 nm, adopting an outer-to-inner path of the ion beam to avoid material re-deposition over the pillar surface. The drift of the ion beam was continuously automatically monitored during milling and corrected if necessary. A series of regular cross-sections was made simultaneously with the ring drilling procedure in order to avoid re-deposition problems over the pillar surface during FIB milling and to provide a more accurate measurement of the actual milling depth after each step. Figs 6(c) and 7(a) illustrate two different steps of the milling procedure for the TiN coating.

A micrograph of one of the realized tests for the Au coating on Silicon substrate is reported in Fig. 7b. In this case, the diameter of the pillar was of the order of 1.5 μm (equal to the coating thickness).

It is important to note that the procedure described above was performed in multiple sessions (i.e. on different days) and at multiple locations on the surface of the coated samples. No less than three implementations of the same procedure were used to obtain the results. In all cases the repeatability and consistency of the results were found to be excellent, i.e. the variation of the results lay well within the estimate of the error based on the statistics of the Digital Image Correlation analysis (see below). The coatings on the samples considered in these studies were nominally uniform. Within the error bound defined by the experimental statistics, no variation of the residual stress across the sample surface was observed.

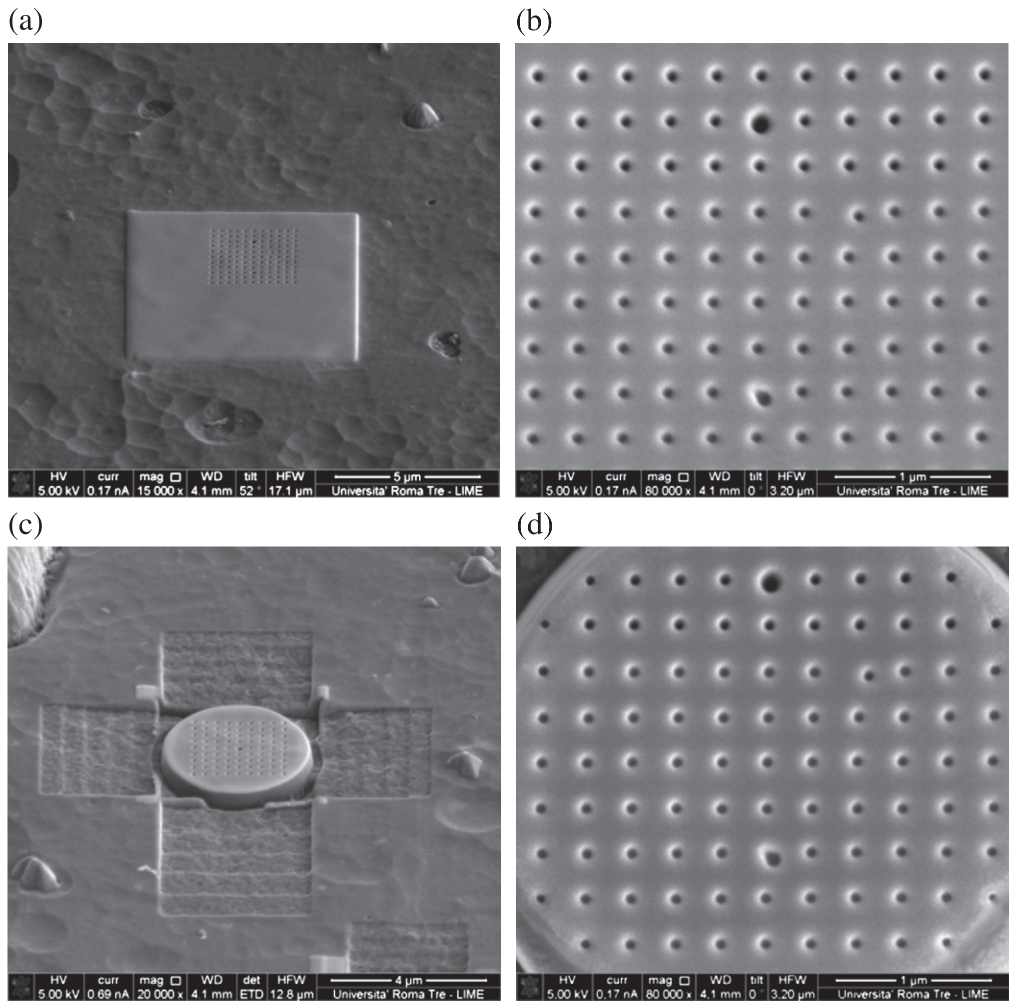

Fig. 6. Illustration of the FIB operations and SEM high resolution imaging steps. (a) Deposition of a Pt (electron beam) 100 nm thick platinum layer and milling of a pattern of very small dots (diameter 50 nm). (b) High resolution SEM imaging of the reference patter before milling. (c) Incremental FIB milling. (d) High-resolution SEM imaging of the reference patter after each milling step.

Based on the results of FEM modeling reported previously, both the maximum milling depth and diameter of the pillars were fixed to be equal to the coating thickness, in order to achieve complete stress relief and at the same time to obtain a sufficiently large surface area unaffected by FIB artefacts for the determination of strain relief.

Fig. 6b–d report the data for the TiN coating showing the initial and the relieved patterns at the sample surface. These images were used as input for the Digital Image Correlation (DIC) analysis of strain relief. It is worth noting that no significant morphological change in the milled dot pattern was observed (note the bigger radius reference dots visible in Fig. 2b–d). Thus, no relevant artefacts due to the FIB milling process (such as re-deposition or surface damage) were induced on upper surface of the pillar.

A cross section of the pillar (Fig. 8) was milled as the final stage of the procedure in order to obtain a complete morphological and microstructural characterisation of the pillar volume, namely, the final milling depth, the actual slope of the pillar, and information about the coating local microstructure, as well as the presence of defects (Fig. 8). The measured actual geometry of the stubs (including lateral slope) was used to create a model for FEM calibration. This allowed obtaining specific calibration curves for each pillar, and also identified the relevant range of geometric parameters needed for sensitivity analysis.

Some re-deposition of TiN is visible on the left-side of the pillar in Fig. 8. This experimental evidence confirms that strain measurement in proximity of the edges is impeded by FIB-induced artefacts, as observed in previously reported attempts to use slot and blind hole geometry [6,7]. This observation confirms the key advantage of the proposed geometry in comparison to the other solutions available in literature, due to the fact that uniform strain relief occurs over a relatively large area substantially unaffected by FIB milling artefacts.

4. Digital image correlation analysis

The Digital Image Correlation (DIC) method of strain determination has undergone rapid development over the last two decades, due to the greatly increased availability of digital systems for imaging across the scales. Alongside scanning electron microscopy, other imaging modalities can be used, including Atomic Force Microscopy (AFM), Scanning Transmission X-ray Microscopy (STXM), and various digital capture methods for optical images. Although conventional strain gauge methods remain widespread in industrial and research use, non-contact image-based strain evaluation methods possess numerous advantages. Perhaps the two most obvious ones are (i) the non-contact nature of this method, and (ii) its scale-independence.

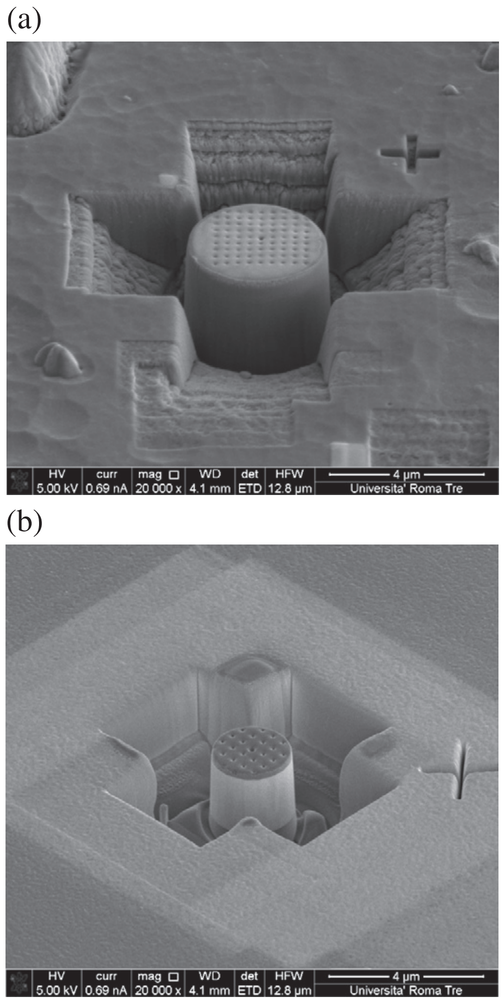

Fig. 7. Illustration of the resulted stress-relieved "stubs" for (a) the TiN coating on WC–Co substrate and (b) the Au coating on silicon substrate.

The principles of DIC in current use are connected with its origins in particle anemometry, where the purpose is to track the motion of particles through an optically observed flow. In solid mechanics applications, particles are replaced with "speckled" surface patches, and their motion is traced. It is necessary to take into account the fact that the tracked patches (sub-regions) may themselves undergo deformation, and thus become different from their reference state. However, the most likely new location of a patch can be found by computing the correlation function between the reference patch image and its various putative displaced versions. The most likely new location (and hence displacement) of the patch is such that delivers the maximum to the correlation function. In other words, the displacements are found as

$$(u^*, v^*) = \arg\ \max C(u, v), \tag{3}$$

where C is the correlation function, u,v denote all possible displacements along the two coordinates in the image plane, and u^*, v^* is the final displacement solution that corresponds to the maximum of the correlation function.

By partitioning the image into multiple patches and repeating this procedure, it is possible to compile a displacement map. This map can be subsequently differentiated numerically to determine strains. Note that sub-pixel accuracy of displacement determination can be achieved [6].

In the present study a Matlab® implementation of the DIC procedure was used, making use of the library function cpcorr. Relative displacement values were found between the reference and milled images for the patches centred on the milled dots in the surface pattern. The calculation was repeated for multiple pairs of milled dots, and the average value of the overall strain was computed. These values of the strain relief observed at different stages of the ring drilling procedure served as the input into the analysis procedure for stress evaluation described in the following section.

5. Residual stress evaluation and validation

An example of the experimentally obtained strain relief profile is presented in Fig. 6 for the TiN PVD coating under investigation, while average relaxation strains at maximum penetration depth (such that $h/d>1$) are reported in Table 1 (average data and error bars are calculated from 6 different tests for both coatings). The magnitudes of strain relief components measured along three different directions at the pillar surface are close, indicating that the residual stress state inside the TiN coating is nearly equi-biaxial. Hence, Hooke's law for equi-biaxial plane stress conditions can be used for the evaluation of average residual stress over the stub. Similar results were also obtained for the PVD Au coating on Si substrate. The measured relief strain values shown in Fig 9 are in close agreement with the numerically predicted curve. Note that, similarly to the curve predicted from FE simulations, the experimental stress relief profile shows a maximum, with a reduction of strain relief and then saturation at higher drilling depths.

The statistical error of the strain relief evaluation by DIC was estimated as follows. The dot pattern deposited on the sample surface contains a large number of dots, as is apparent from the micrographic images (Fig. 6). The comparative analysis (between deformed and reference image) of the spacing for each pair of dots provides a means of strain evaluation. In this way, a statistically representative array of strain values (typically >10) can be obtained for each stage of trench milling. The standard deviation of the strain value within this array was taken as a measure of the nominal strain error.

The average in-plane strain relief values were also calculated by fitting the FEM-simulated relief curve reported in the first part of this report to the experimental strain data, using the elastic modulus of the coating measured by nano-indentation and assuming Poisson's ratio from literature. Some of the FEM models used in this study

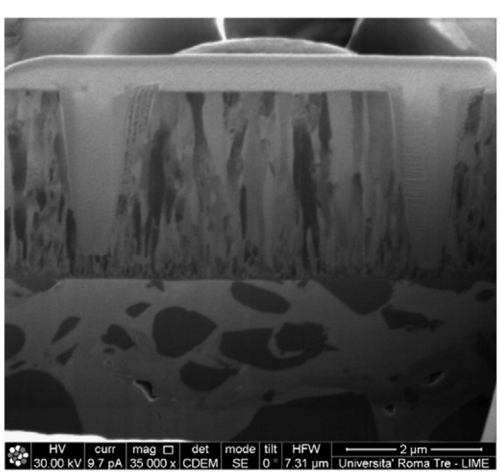

Fig. 8. Illustration of the geometry of the FIB-milled "stub". Lateral slope is lower than 5°. A large number of grains is involved in the relaxation strain process during material removal.

Table 1
Results of stress calculation for both PVD coatings under investigation. Comparison between analytical calculations (Eq. 1) and FEM modeling with slope of the stub.

	Au coating on Si substrate	TiN coating on WC–Co substrate
Measured relaxation strain at maximum depth ($h/d>1$)	-0.002 ± 0.0006	0.092 ± 0.0008
Residual stress, analytical (Eq. (1)) [MPa]	$+261.2\pm85.5$	-6162.0 ± 530.0
Residual stress, FEM modeled with slope [MPa]	No relevant slope detected	-6046.0 ± 514.0
Residual stress, Independently measured [MPa]	+280 (curvature method)	−5840 (XRD, $\sin^2\psi$, σ_φ)

incorporated real geometry reflecting the actual slope of the stub, as directly evaluated in situ by SEM after FIB milling.

As reported in Table 1, in the case of the TiN coating the results of the FEM simulation were slightly different from the analytical ones, essentially due to the actual slope of the remaining stubs being of the order of 2°.

A further possible source of disagreement may be the systematic error in the determination of the surface position from which the trench depth is measured. In order to address this issue, the fitting procedure using the master curve function was repeated, but with the allowance for a shift of the zero-depth position. The result is shown in Fig 10.

Note that allowing for the zero-depth shift results in a slightly higher value of relief strain. Although the two results obtained are statistically in agreement, the zero-depth correction improves the quality of fit and results in a smaller error (<2%) in the determination of the complete strain relief, and hence of the residual stress (compared to about 4% otherwise).

In the case of the Au coating, no significant slope of the pillars was measured, and stress calculation results by the analytical procedure and FEM were essentially coincident.

On the basis of six repeated tests carried out for both coatings, the values of residual stresses in the coatings were found to be equal to -6.04 ± 0.51 GPa for the CAE-PVD TiN coating and $+261.2\pm85.5$ MPa for the DC sputtered Au coating, as reported in Table 1. These results are in good agreement with the estimates obtained by XRD analysis: −5.84 GPa for the TiN coating (using the same elastic constants) and 280 MPa for the Au coating (by curvature measurement). Note also that XRD data analysis contained a greater uncertainty due to the strong texture of the TiN coating (Fig. A5).

Although the result for the compressive stress in the TiN coating appears to be very large, it is not unusual to encounter such values in the literature for strong ceramic systems, such as TiN [19,20]. In contrast, the residual stress magnitude for the metallic Au coating is quite low. Nevertheless, the method provides a good estimate of the residual stress value, compared to independent measurement by a different technique [21].

Fig. 11 presents the calculated stress–depth profiles [4,13] for the TiN coating for the case of five calculation steps (Eq. (A5), after FEM evaluation of influence coefficients), showing that the compressive equi-biaxial residual stress increases towards the coating/substrate interface. This deduced stress gradient can be correlated with the TiN

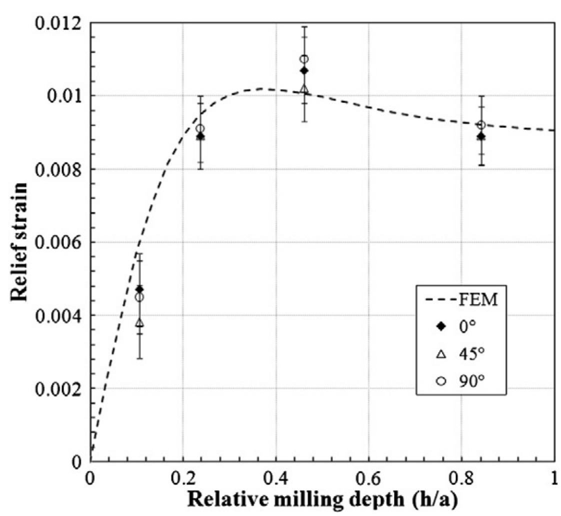

Fig. 9. Experimentally measured relaxation strain on the TiN coating and fitting with the finite element modeling prediction.

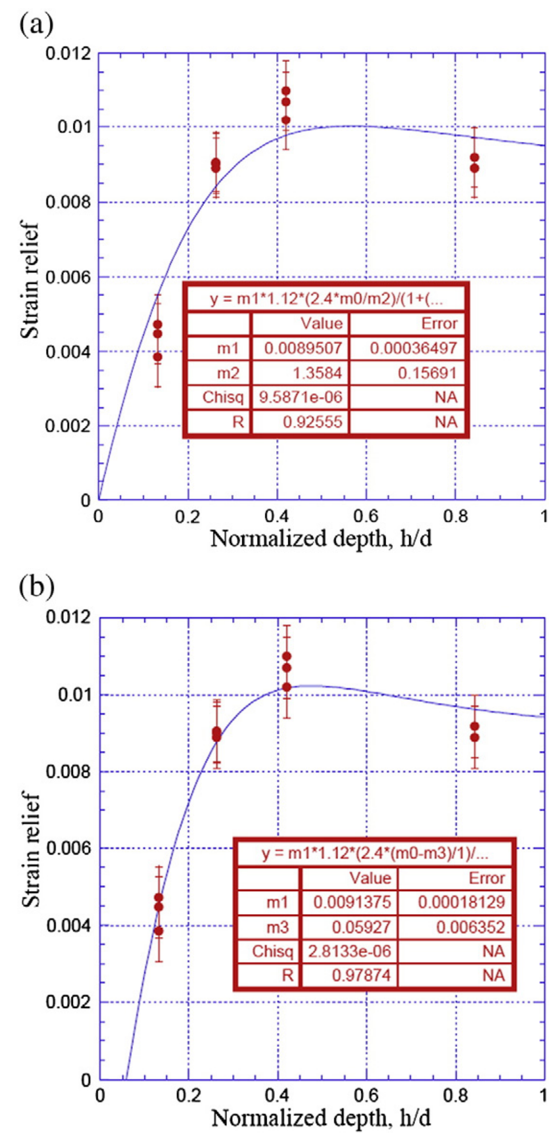

Fig. 10. The evaluation of complete strain relief (a) by master curve fitting, and (b) by master curve fitting with zero-depth shift.

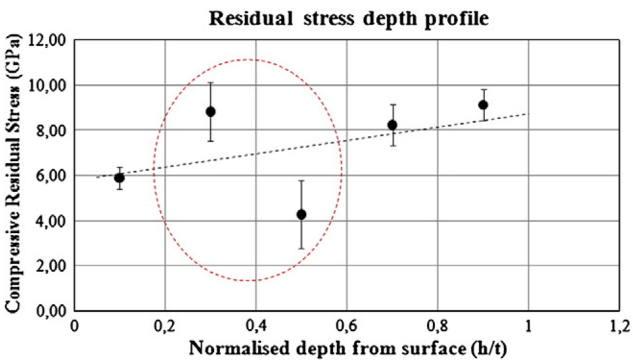

Fig. 11. Depth profiling of residual stress for the TiN coating.

coating microstructure illustrated in Fig. 5(a) and Fig. 8. Coarser columnar grains are observed in the near-surface regions, while a much finer microstructure is evident near the coating/substrate interface. Progressive reduction of the intrinsic stresses is therefore likely to occur during film deposition, as a consequence of columnar grain growth.

Other possible explanations could be put forward for the observed small disagreement between the experimentally measured strain values and the FEM predicted relaxation curve (Fig. 9), e.g. the inhomogeneity of stress within the coating layer.

Finally, it is important to note that some inaccuracies in the stress profile evaluation highlighted in Fig. 11 are due to the uncertainties in the actual trench depth measurement. These uncertainties are related to the high surface roughness of the TiN PVD coating analysed. Noting the steep slope of the relief curve for the pillar geometry at low milling depths, a significant error in stress evaluation close to the surface may arise even due to relatively small errors in the depth measurement. Note, however, that the obtained stress gradient is in good agreement with the microstructural observations and with other XRD stress profiles for thin coatings reported in the literature [16,17].

Further studies are now ongoing to evaluate the optimal geometrical configuration (i.e. diameter of the pillar and maximum drilling depth with respect to coating thickness and surface roughness) for the analysis of stress gradients in thin coatings.

Another microstructural effect to be considered is represented by the grain-boundary residual stresses that are known to develop in the first stages of the growth phase [13,14]. It is known from the literature that a columnar grain structure can give a tensile residual stress state at the grain boundaries: this stress component could remain incompletely relaxed after FIB milling, but is not accounted for in a homogeneous FE model. However, the tensile stress component at grain boundaries is known to be always significantly lower than the stress components coming from surface ion bombardment and thermal expansion mismatch between coating and substrate.[13,14]

At this point, some further discussion is necessary of the assumptions adopted during modeling. The adoption of Eq. (1–2) and all modeling activities for stress calculation are based on the assumptions that (1) the elastic properties of the analyzed coating is homogeneous and isotropic and (2) that continuum mechanics remains valid at the considered scale.

An SEM micrograph of the TiN coating is reported in Fig. 5(a). A strong columnar microstructure is evident. This indicates that some inaccuracies in stress calculation could arise as a consequence incorrect estimation of the actual anisotropic elastic constants of the coating.

Nevertheless, the FEG-SEM cross section of the stress relieved pillar (Fig. 8) also shows that the average size of the pillar is usually much greater than the average grain size of the coating. In addition, the evaluation of elastic modulus by nano-indentation also gives an average over a large number of grains.

Therefore, the assumption of isotropic elastic behaviour for the coating could be defended as a reasonable choice, at least at the scale considered, where grain boundaries do not play a significant role in the mechanical deformation process.

It is important to note also that the use of similar elastic constants and gauge volumes guarantees the consistency between residual stress values measured by the XRD-$\sin^2\psi$ and nano-indentation method.

6. Discussion and conclusions

In the present report we presented a new methodology for residual stress determination at the micro-scale by the combination of FIB ring drilling, SEM imaging, DIC strain analysis, and FEM simulation of stress–strain relief in residually stressed surfaces. The results of stress evaluation in two different coated systems were presented, and a good agreement was found with the estimates obtained by other conventional techniques. In both cases, nearly equi-biaxial stress states were observed. In addition, an estimation of the stress gradient through the coating thickness was shown to be possible, although further work is required in this respect, and is ongoing. The present study contains some significant developments over the existing state-of-the-art.

The ring-core milling geometry chosen in the present approach has been shown (through reasoning and numerical simulation) to be uniquely effective in providing complete, biaxial, substantially uniform surface strain relief over significant areas available for microscopic imaging. This is a fundamental improvement over previous attempts, where steep strain gradients were created during the milling experiment. Moreover, in previous studies the greatest strain relief values invariably arose close to the milled trenches, where surface damage and modification occurred during milling, thus preventing accurate strain determination.

The combination of FIB milling and SEM imaging within a single experiment ensures the ease and efficiency of use of the present method, since it does not require the laborious and time-consuming transfer of samples between instruments. In fact, the current procedure can be successfully automated for systematic batch mode residual stress mapping across significant areas.

Finite element simulations were carried out of the strain relief caused by ring drilling in residually stressed surfaces, showing that complete stress relief is achieved for $h/d \geq 1$, thus allowing to directly evaluate the average residual stress from the measured strain with no need of FEM simulations.

A number of other interesting peculiarities were also observed, such as the steep, approximately linear dependence of the strain relief on the milling depth at low penetrations, followed by a maximum and subsequent reduction to a constant value. The observation of this behaviour offers new insight that can be effectively used to develop improved, more precise depth-resolving stress evaluation procedures.

The approach can be readily generalised to the analysis of non-equi-biaxial residual stress states, since the DIC evaluation of strain relief in multiple directions can be readily extracted from microscopic images. The present paper thus provides an in-depth, detailed description of the method that we now propose to call "micro-ring-core" (MRC) [22]. The principal advantage of this technique over previously reported approaches is its ability to determine local residual stresses in (poly)crystalline and amorphous materials at micron and sub-micron scales.

Acknowledgements

Authors would like to acknowledge Daniele De Felicis for technical assistance during FIB analyses, performed at the interdepartmental laboratory of electron microscopy of university of Roma Tre, Rome Italy (http://www.lime.uniroma3.it), and Prof. Laura Depero (University of Brescia) for XRD residual stress measurements.

Appendix A. Details of the FEM developed procedure for average stress and stress gradient analysis on thin coatings by the incremental ring-core method

Let Cartesian axes x and y be associated with the sample surface, and axis z with the surface normal. Since at the sample surface the tractions vanish, the out-of-plane normal stress $\sigma_z = 0$.

One of the most widely used approaches to the study of surface relaxation strain after incremental material removal is represented by the integral method proposed by Schajer [4] for the hole drilling geometry and generalised to the ring-core geometry by Ajovalasit et al. [13]

In this approach, the measured strain relief $\varepsilon(h)$ in a particular radial direction over the surface of the stub due to a trench of depth h is given by the integral of the infinitesimal strain relief components due to the removal of tractions at all depths in the range $0 \le H \le h$:

$$\Delta\varepsilon(h) = \int_0^h \{A(H,h)[\sigma_1(h) + \sigma_2(h)] + B(H,h)[\sigma_1(H) - \sigma_2(H)]\cos 2\alpha_k(H)\}dH \quad \text{(A1)}$$

Here $\Delta\varepsilon(h)$ is the strain relieved as measured at the surface after milling to depth h, $\sigma_1(H)$ and $\sigma_2(H)$ are the residual principal stresses acting at depth H, α is the angular coordinate measured anticlockwise from the maximum principal stress direction to the measuring direction, and $A(H, h)$, $B(H, h)$ are the influence functions, which are usually determined by finite element modeling. If the milling is divided into n finite increments, Eq. (A1) can be written as follows:

$$\Delta\epsilon_n = \sum_{i=1}^{n} A_{ni}(\sigma_{1i} + \sigma_{2i}) + \sum_{i=1}^{n} B_{ni}(\sigma_{1i} - \sigma_{2i})\cos 2\alpha_i \quad \text{(A2)}$$

where σ_{1i} and σ_{2i} are the residual principal stresses in the i^{th} layer and α_i is the angle from the stress σ_{1i} to the measuring direction, A_{ni}, and B_{ni} are the influence coefficients which relate the strains relaxed at the surface when the groove has n depth increments to the principal stresses acting in the i layer.

Residual stress can be therefore evaluated after calculation of the two matrices of calibration coefficients A_{ni}, and B_{ni}, which is usually performed by finite element modeling [13].

In the case of macroscopic hole drilling and ring-core methods, relaxation strain measurement is usually performed along three different radial directions (e.g. by a strain gauge rosette), in order to determine all in-plane stress components.

Note also that the influence functions, when expressed in the form of Eqs. (1–2), also depend on material properties.

To evaluate the coefficient A_{ni}, it is sufficient to consider an axisymmetric model subjected to an hydrostatic calibration stress field ($\sigma_1 = \sigma_2$ in Eq. (A2)), so the coefficient A_{ni}, can be calculated as:

$$A_{ni} = \frac{\Delta\varepsilon_{ni}}{2\sigma_1} \quad \text{(A3)}$$

On the other hand, calibration coefficient B_{ni}, can be obtained by imposing a pure shear calibration stress field ($\sigma_2 = -\sigma_1$ in Eq. (A2)), by:

$$B_{ni} = \frac{\Delta\varepsilon_{ni}}{2\sigma_1} \quad \text{(A4)}$$

Coefficients B_{ni} are also calculated by an axisymmetric FEM model, by using axisymmetric elements which also admit non-axisymmetric loading [13,14].

In case of equi-biaxial residual stress field (i.e. $\sigma_{1i} = \sigma_{2i} = \sigma_i$, at any given depth from surface), Eq. (A2) reduces to:

$$\Delta\epsilon_n = \sum_{i=1}^{n} 2A_{ni}\cdot(\sigma_i) \quad \text{(A5)}$$

In this case, only coefficients A_{ni} need to be determined.

This situation is particularly relevant to the case of residual stress analysis in thin coatings on flat substrate, where an equi-biaxial stress state is usually expected due to the uniform growth of the film [15].

Previous studies [13] have shown that, at a fixed maximum depth, the errors in stress calculations depend on the amount and on the distribution of the n calculation increments, with the optimal steps sequence obtained by imposing the condition $A_{nn} = \text{const}$ [13,14].

In this work, commercial finite element analysis package ANSYS 9.0 was used for the FEM analysis of relaxation strains after FIB drilling of annular trenches over a residually stressed surface. An axisymmetric model was created consisting of a stiff residually stressed coating on a dissimilar substrate.

Fig. A1 illustrates some of the cylindrical models meshed using quadratic temperature–displacement axisymmetric elements (Plane83 in ANSYS, which also allow non-axisymmetric loading for calculation of influence coefficients B_{ni}) representing a coating layer and a substrate block. The calibration coefficient matrices A_{ni} and B_{ni} can be therefore calculated by applying in the model a unit pure in-plane biaxial stress and a pure shear calibration stress, and the use of Eqs. (A3) and (A4), respectively [4,13].

The incremental ring drilling process is simulated by the progressive removal of elements and illustrated in Fig. A2 for the case $n = 3$, where the applied calibration pressures are shown. The diameter of the remaining stub (d) was fixed equal to coating thickness t, so that $d/t = 1$.

The material properties of both coating and substrate were varied in order to reproduce the most commonly encountered situations in case of thin coatings. The ratio of elastic moduli between coating and substrate (E_c/E_s) was varied from 0.1 to 100 (0.1, 1, 10, and 100), while the Poisson ratios of both the coating and substrate (ν_c, ν_s) were varied from 0.25 to 0.35 (0.25, 0.30, and 0.35), for a total of 36 realized models.

The influence of the lateral slope of the stub (which is likely to happen in case of FIB milling) was also considered via the development of specific models (see Fig. A3).

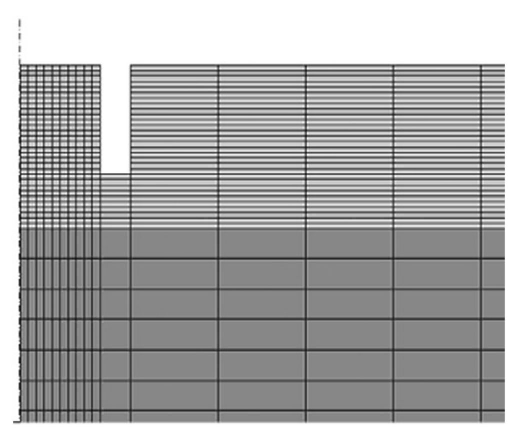

Fig. A1. Detail of the axisymmetric FEM model of the ring drilling procedure: step 20 of 30.

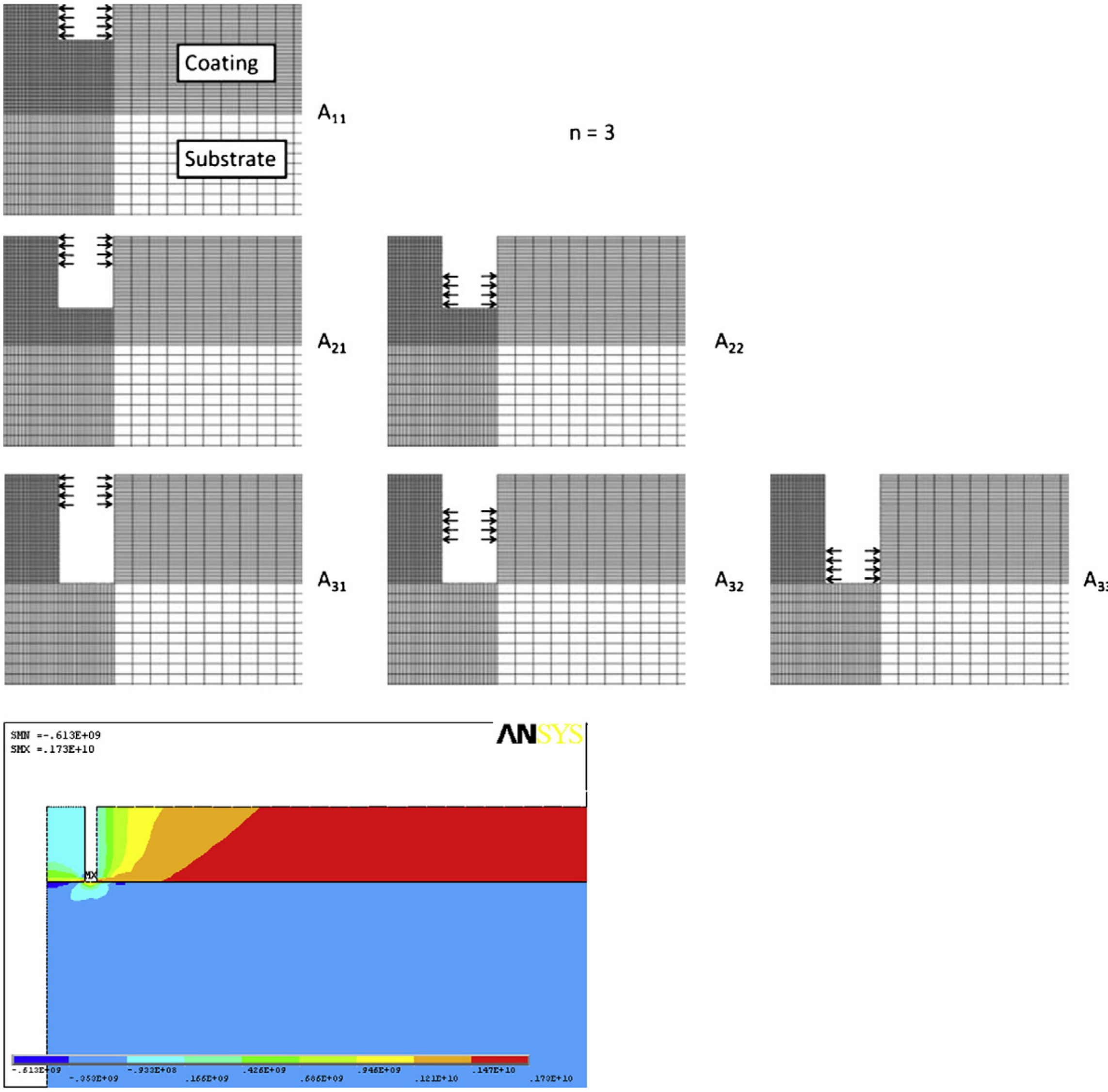

Fig. A2. Illustration of Finite Element simulation steps for the through-thickness stress profile evaluation. Countour plot (FEM) of the stress rearrangement after ring-drilling on a residually strerssed surface. It is worth noting that the upper surface of the remaining pillar is completely stress releived if h/d >1.

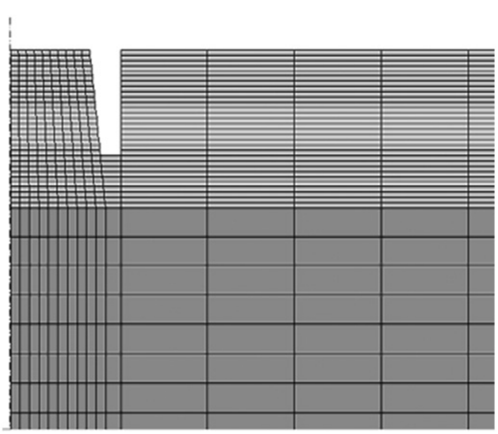

Fig. A3. Detail of the axisymmetric FEM model with arbitrary slope: step 20 of 30.

References

[1] J.-S. Chung, G.E. Ice, J. Applied Physics 86 (1999) 5249.
[2] B.C. Larson, W. Yang, G.E. Ice, J.D. Budai, J.Z. Tischler, Nature 415 (2002) 887.
[3] P.J. Withers, H.K.D.H. Bhadeshia, Mater. Sci. Technol. 17 (2001) 355.
[4] G.S. Schajer, J. Eng. Mater. Technol. 110 (1988) 338.
[5] H. Du, H. Xie, Z. Guo, B. Pan, Q. Luo, C. Gu, H.C. Jiang, L.J. Rong, Opt. Lasers Eng. 45 (2007) 1157.
[6] N. Sabaté, D. Vogel, A. Gollhardt, J. Keller, C. Cané, I. Gràcia, J.R. Morante, B. Michel, Micromech. Microeng. 16 (2006) 254.
[7] N. Sabaté, D. Vogel, A. Gollhardt, J. Marcos, I. Gràcia, C. Cané, B.N. Michel, Nanotechnology 17 (2006) 5264.
[8] A.M. Korsunsky, S. Cherian, R. Raiteri, R. Berger, Sens. Actuators, A 139 (2007) 70.
[9] S. Massl, J. Keckes, R. Pippan, Acta Mater. 55 (2007) 4835.
[10] G.S. Schajer, M.B. Prime, ASME Journal of Engineering Materials and Technology 128 (2006) 375.
[11] A.M. Korsunsky, J. Mech. Phys. Solids 43 (1995) 1221.
[12] R.J.H. Paynter, D.A. Hills, A.M. Korsunsky, Int. J. Solids Struct. 44 (2007) 6653.
[13] G.S. Schajer, J. Eng. Mater. Technol. 110 (1988) 338.
[14] A. Ajovalasit, G. Petrucci, B. Zuccarello, J. Eng. Mater. Technol. 118 (1996) 224.
[15] E. Bemporad, M. Sebastiani, F. Casadei, F. Carassiti, Surf. Coat. Technol. 201 (2007) 7652.
[16] W.C. Oliver, G.M. Pharr, J. Mater. Res. 7 (1992) 1564.
[17] M. Gelfi, E. Bontempi, R. Roberti, L.E. Depero, Acta Mater. 52 (2004) 583.
[18] G.G. Stoney, Proc. R. Soc. Lond. A 82 (1909) 172.
[19] G.C.A.M. Janssen, Thin Solid Films 515 (2007) 6654.
[20] R. Daniel, K.J. Martinschitz, J. Keckes, C. Mitterer, Acta Mater. 58 (2010) 2621.
[21] G. Chen, D. Singh, O. Eryilmaz, J. Routbort, B.C. Larson, W. Liu, Appl. Phys. Lett. 89 (2006) 172104.
[22] A.M. Korsunsky, M. Sebastiani, E. Bemporad, Mater. Letters 63 (2009) 1961.